Modern radio engineering and telecommunication systems

Современные радиотехнические и телекоммуникационные системы

UDC 537.874+537.877+621.37
https://doi.org/10.32362/2500-316X-2026-14-4-96-105
EDN TAFVVJ

RESEARCH ARTICLE

Tracking-based formation of vector radio images

Sergey S. Shadinov @,
Mihail S. Kostin

MIREA – Russian Technological University, Moscow, 119454 Russia
@ Corresponding author, e-mail: shadinov@mirea.ru

• **Submitted:** 26.12.2025 • **Revised:** 06.02.2026 • **Accepted:** 26.05.2026

Abstract
Objectives. The aim of this article is to investigate the possibility of forming vector radio images of small-size objects (SSO) using a digital vector network analyzer (VNA) with a controllable bandwidth and frequency step of the tracking generator.
Methods. The work is based on the comprehensive application of the following methods: analysis of radio wave processes in the context of radio vision, the apparatus of *N*-pole theory, numerical methods of statistical radio engineering, and computer modeling (including both electromagnetic and functional-block simulation).
Results. A new method for vector tracking-formation of signal radio images of SSO has been developed. Its fundamental difference from traditional pulsed methods of near-field radio vision lies in the use of an *S*-parametric model of a spatial *N*-pole to describe the inhomogeneous medium, as opposed to approaches based on scalar signal transformation. To analyze the accuracy of the method, a model of operator ψ-transformation has been proposed, allowing for the evaluation of projective distortions in vector radio images of SSO signatures. Verification of the method was carried out on a custom-developed software-hardware complex based on the R&S ZNLE6 VNA. The complex provides coherent processing and verification of signal radio images of SSOs recorded under the influence of non-fluctuating interference.
Conclusions. During the research, a method for vector tracking-based formation of radio images with spectro-temporal unfolding of the power spectral density function was proposed. This method is free from the limitations of pulsed analogs and can be used as one of the solutions for verifying SSO in near-range radio vision. The foundation of the proposed method can be a model of an inhomogeneous medium as a spatially-oriented system of coupled *N*-poles, described by *S*-parameters. The practical effectiveness has been experimentally confirmed: the probability of verifying a SSO reaches at least 0.94 (Neumann–Pearson criterion) with a signal-to-noise ratio ⩾15 dB and a signal-to-interference ratio ⩾9 dB. These results are of practical value for the development of near-field radio vision technologies.

Keywords: vector radio image, radio identification, small-size object, object signature, radiogenome

For citation: Shadinov S.S., Kostin M.S. Tracking-based formation of vector radio images. *Russian Technological Journal.* 2026;14(4):96–105. https://doi.org/10.32362/2500-316X-2026-14-4-96-105, https://elibrary.ru/TAFVVJ

Financial disclosure: The authors have no financial or proprietary interest in any material or method mentioned.

The authors declare no conflicts of interest.

НАУЧНАЯ СТАТЬЯ

Трекинг-формирование векторных радиоизображений

С.С. Шадинов @**,**
М.С. Костин

МИРЭА – Российский технологический университет, Москва, 119454 Россия
@ *Автор для переписки, e-mail: shadinov@mirea.ru*

• **Поступила:** 26.12.2025 • **Доработана:** 06.02.2026 • **Принята к опубликованию:** 26.05.2026

Резюме
Цели. Целью статьи является исследование особенностей формирования векторных радиоизображений малоразмерных объектов (МРО) при помощи цифрового векторного анализатора цепей (ВАЦ) с управляемыми полосой и шагом перестройки частоты трекинг-генератора.
Методы. Работа основана на комплексном применении следующих методов: анализ радиоволновых процессов в контексте радиовидения, теория *N*-полюсников, численные методы статистической радиотехники и компьютерное моделирование (включая электродинамическое и функционально-блочное).
Результаты. Разработан новый метод векторного трекинг-формирования сигнальных радиоизображений МРО. Его принципиальное отличие от традиционных импульсных методов ближнего радиовидения заключается в использовании *S*-параметрической модели пространственного *N*-полюсника для описания неоднородной среды вместо подходов, основанных на скалярном сигнальном преобразовании. Для анализа точности метода предложено операторное Ψ-преобразование, позволяющее оценить проекционные искажения векторных радиоизображений сигнатур МРО. Верификация метода осуществлена на созданном программно-аппаратном комплексе на базе ВАЦ R&S ZNLE6 (производитель – Rohde & Schwarz, Германия). Комплекс обеспечивает согласованную обработку и верификацию сигнальных радиоизображений МРО, регистрируемых в условиях воздействия нефлуктуационных помех, а также аддитивного белого гауссовского шума.
Выводы. В ходе исследования предложен метод векторного трекинг-формирования радиоизображений со спектрально-временной разверткой функции спектральной плотности мощности, свободный от ограничений импульсных аналогов, который может быть использован в качестве одного из решений верификации МРО в ближнем радиовидении. Основой предложенного метода может служить модель неоднородной среды как пространственно-ориентированной системы связанных *N*-полюсников, описываемой *S*-параметрами. Практическая эффективность подтверждена экспериментально: вероятность верификации МРО достигает не менее 0.95 (критерий Неймана – Пирсона) при отношении сигнал/шум ⩾15 дБ и отношении сигнал/помеха ⩾9 дБ. Результаты представляют практическую ценность для развития технологий ближнего радиовидения.

Ключевые слова: векторное радиоизображение, радиоидентификация, малоразмерный объект, сигнатура объекта, радиогеном

Для цитирования: Шадинов С.С., Костин М.С. Трекинг-формирование векторных радиоизображений. *Russian Technological Journal*. 2026;14(4):96–105. https://doi.org/10.32362/2500-316X-2026-14-4-96-105, https://elibrary.ru/TAFVVJ

Прозрачность финансовой деятельности: Авторы не имеют финансовой заинтересованности в представленных материалах или методах.

Авторы заявляют об отсутствии конфликта интересов.

INTRODUCTION

The signal verification process in short-range radio vision systems designed for small-sized objects (SSOs) is influenced by several factors. Key aspects include the selection of authenticators, system configuration, and post-processing algorithms. Since the authenticators that define the object's properties manifest as specific deformations in its scattered field spectrum, the primary step in creating a radio image involves analyzing the reflected field structure and identifying features within the radio signal image. For probing purposes, either a pulse signal or a signal with a linearly varying power spectral density (PSD) function can be employed [1].

The use of signals having a gradual (linear) frequency-time sweep has advantages over the classical pulse method. These include high stability of signal phase synchronization, flexible vector and scalar scaling, the ability to selectively analyze the object's response to different frequencies while suppressing interference, high matched filtering efficiency, and the ability to adapt the shape of the probing signal to the object's specified impulse response (IR) [2].

The relevance of the study consists in the potential use of the described method to construct SSO radio images in complex, dispersive, reactive, and nonlinear environments.

Since the material environment and the radio vision object that generate complex radiophysical distortions can be considered as an *N*-pole with an *S*-matrix, the proposed technique takes into account the contribution of each harmonic to the synthesized radio image in accordance with a given feature cluster. Consequently, vector tracking-based formation of radio images with spectral-temporal resolution becomes an efficient solution for noise-resistant short-range radio vision, ensuring the effective detection and verification of SSO signal radio images in the presence of non-fluctuating interference and noise [3].

While traditional radio vision systems utilize scalar signals, such as ultrashort or linearly modulated radio pulses, vector signals, which are represented by an array of amplitudes and phases, allow the temporal profile of a radio image to be reconstructed using a polynomial. By controlling the frequency tuning step of the tracking generator, compressed spectral sensing techniques can be applied to reduce the number of measurements per sample while maintaining information. This presents new opportunities for addressing radio vision challenges, including those related to priority radio guidance systems [4]. This paper therefore proposes generating vector radio vision signals in the form of *S*-parameters from a heterogeneous environment. The proposed *S*-parameter method offers several benefits, including the ability to facilitate the radio identification of small objects in the presence of noise and non-fluctuating interference based on the coherent reception of the radio vision signal. Several studies conducted by foreign researchers have demonstrated the need for in-phase reception using MIMO SAR[1] technology when processing deflated radio images [5]. Most research in the field of radio vision focuses on 2D visualization methods for radio images of objects [6], based on multi-position scanning [7]. The method proposed in the present paper enables the generation of signal radio images in a single-position configuration without raster scanning by obtaining an S_{21} vector profile [8].

1. *S*-PARAMETRIC *N*-POLE SYSTEM CORRESPONDING TO SSO

The proposed method involves representing SSO and its surrounding environment (the scene) as an *N*-pole system. This system can be analyzed using the theory of *N*-poles and *S*-parameters. The example of a quadcopter-type SSO, whose radio signatures are analyzed further in this paper, are shown in Fig. 1.

Fig. 1. Quadcopter-type SSO when capturing a radio image

In this case, the non-uniform system consists in a four-pole network comprising two antennas connected to a vector network analyzer (VNA) and the SSO. This network is defined by a radio image derived from the parameter , which can be described by the following analytical expression:

$$\dot{S}_{21} = \frac{\dot{U}_{\mathrm{Ref}}(n)}{\dot{U}_{\mathrm{Tx}}(n)}, \quad (1)$$

where $\dot{U}_{\mathrm{Ref}}(n) = \sum_{n=1}^{N}\sum_{m=1}^{M} k_n A_{\mathrm{Tx}} \exp(j(\omega_n t + \varphi_{nm})) * h_{\mathrm{a}} * h_{\mathrm{Env}}$ is the signal received after being scattered by the

[1] Multiple Input Multiple Output Synthetic Aperture Radar is a combination of two technologies: MIMO (Multiple Input Multiple Output), which uses multiple input and output transmission channels; and SAR (Synthetic Aperture Radar), which employs a synthetic aperture antenna.

SSO signature; $\dot{U}_{\text{Tx}}(n)=\sum_{n=1}^{N} A_{\text{Tx}} \exp(j(\omega_n t+\varphi_n)) * h_\text{a}$ is the transmitted signal; A_{Tx} is the signal amplitude; $\omega_n = 2\pi f_n$ is an angular frequency of the nth harmonic of the synthesized radio vision signal; φ_n is the phase of the nth harmonic; h_a is the antenna IR; h_{Env} is the environment IR; $N = 200$ is the number of harmonics in the synthesized signal; M is the number of elementary reflecting planes forming the instantaneous signature of the object; * is mathematical convolution; and k_n is the attenuation decrement specified for each discrete value of the formant as follows:

$$k_n = \sqrt{\frac{P_{\text{Tx}} D_1 D_2 \lambda_n^2}{(4\pi R)^2}}, \tag{2}$$

where P_{Tx} is the power of the tracking signal formant; λ_n is the wavelength of the nth harmonic of the synthesized signal; D_1 and D_2 are directivity coefficients of the transmitting and receiving antennas, respectively; and R is the distance from the transmitting antenna to the signal reception point.

The discrete variation in the frequency of the synthesized signal within a given range is described by summation over n in (1), while its interaction with the SSO is described by summation over m. However, despite the presence of phase information in (1), fundamental ambiguity arises in the form of phase uncertainty. In the absence of attenuation, adding a phase component that is a multiple of 2π to the sum does not alter the value of the entire expression.

Therefore, to verify the SSO, it is necessary to capture and process radio images of SSO signatures (that is, radio images of the SSO at a specified angular position) in order to create a database of reference radio images. In this case, the size of the sample and the accuracy of the database determine the probability of recognition according to a given SSO verification criterion.

2. OPERATOR-BASED Ψ-TRANSFORM OF VECTOR RADIOIMAGES

Several studies by foreign researchers have proposed a method for compensating for amplitude attenuation of the radio vision signal in order to correct distortions in the resulting radio images [9]. The amplitude-phase operator presented in the present paper compensates for distortions in radio images caused by the linear displacement of an object perpendicular to the radio vision antenna. Since slight fluctuations on the order of the wavelength lead to significant distortion of radio images, the position of the SSO relative to the antenna array is an important parameter when recording radio images of SSO signatures [10]. Due to the labor-intensive nature of recording SSOs at a multitude of distances from the antenna array, a Ψ-transformation operator is proposed, which uses amplitude and phase operators to significantly reduce the required number of SSO reference radio images. The amplitude operator, $\text{A}\{\cdot\}$, which models natural radio wave attenuation, is defined by a set of coefficients calculated using attenuation decrement (2). The phase operator $\Psi\{\cdot\}$ determines the phase shift for each nth harmonic component of the tracking signal. The initial distance from the SSO to the antenna's phase center is F, while the wavelength λ_1 for the harmonic with frequency f_1 is defined as c/f_1, where c is the speed of light. Each mth elementary plane of the object contributes its own phase contribution, φ_m, upon signal reflection. Thus, the resulting phase φ_n for the nth harmonic with frequency f_n consist in the superimposition (sum) $\varphi_n = \varphi_{m=1} + \varphi_{m=2} + \ldots + \varphi_{m=M} = \sum_{m=1}^{M} \varphi_m$ of all these contributions. The general geometry of the problem for an arbitrary distance F is shown in Fig. 2.

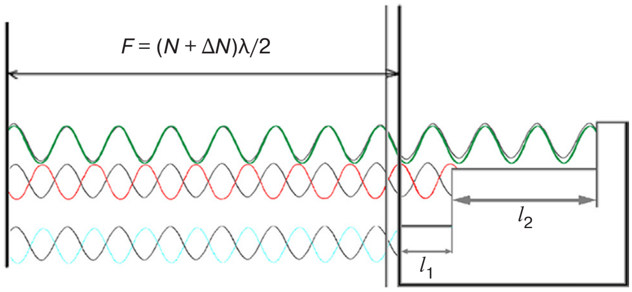

Fig. 2. Harmonics reflected from the SSO elementary planes; l_1 and l_2 are distances between planes in the SSO signature

For a harmonic with frequency f_n, the distance F is a multiple of the wavelength ($F = N\lambda_n$). Since the phase factor $2\pi N$ is an integer that does not alter the value of the total phase φ_n, it can be omitted. Consequently, the phase φ_n, which is determined by the object's geometry (i.e., the arrangement of the elementary planes), is invariant to the term $2\pi N$ and thus provides information about the SSO shape.

Consider the displacement and corresponding distortion of the signature of a radio vision object located at a distance of $F + \Delta F$ (Fig. 3).

In this case, the displacement is defined as $\frac{\lambda}{2}(N+\Delta N)+\frac{\lambda}{2}(N_1+\Delta N_1)$, where ΔN_1 is the residual displacement for the distance ΔF, $\Delta N = \frac{\varphi}{2\pi} \le 1$, while $\varphi = \Delta N 2\pi$ is the phase at the initial distance F. The additional phase at the new distance $F + \Delta F$ for each elementary plane of the object is then defined as $\Delta\varphi = \Delta N_1 2\pi$. The resulting phase is defined as $\varphi_n = \sum_{m=1}^{M} \varphi_m + M\Delta\varphi$. The number of elementary planes M into which the topology of the SSO surface is divided is not a fixed parameter. Rather, its value depends on the signal frequency range: as the wavelength decreases (i.e., as the frequency increases), smaller surfaces are analyzed, leading to an increase in M. Figure 4 illustrates this dependence.

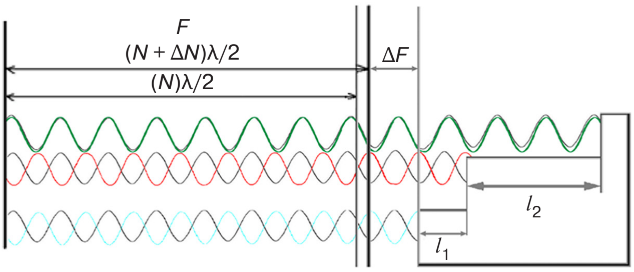

Fig. 3. Reflection from the SSO topological inhomogeneities for the harmonic when the distance changes by ΔF

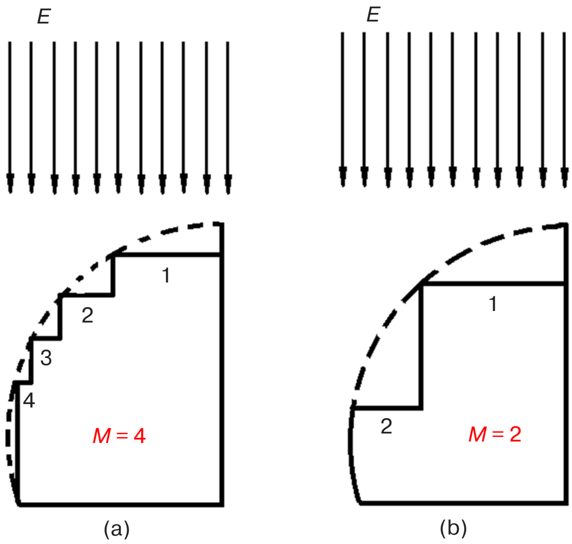

Fig. 4. Discretization of the MRO surface at different wavelengths ($\lambda_1 > \lambda_2$); (a) $\lambda_1 = c/f_1$; (b) $\lambda_2 = c/f_2$; E is intensity of the incident electric field

Since the synthesized probe signal consists of a sum of harmonics that are separated in time, the number of elementary planes M is a function of frequency. The value of M is calculated for each spectral component f_n according to its wavelength [11]. Thus, for the nth harmonic of frequency f_n, we denote the number of planes considered as M_n.

Since the value of $\Delta\varphi M_n$ usually exceeds 2π, the remainder from the division $\Delta\varphi_R = \frac{\Delta\varphi M_n}{2\pi R}$, where R is an integer, is important. The resulting phase when the object is located at a distance $F + \Delta F$ from the antenna array is therefore $\varphi_n = \sum_{m=1}^{M} \varphi_m + \Delta\varphi_R$.

The value of the elementary plane M_n for the nth harmonic is directly proportional to its wavelength, while the number of M_n increases as the frequency rises. Therefore, the frequency grid $\{f_n\}$ specified by the algorithm uniquely determines the corresponding set of values $\{M_n\}$. To perform the calculation, it is sufficient to determine the base value M_1 from the low-dimensionality condition at frequency f_n.

Although the implemented method does not allow for the direct measurement of the parameter M_n, it is possible to record the number of phase jumps corresponding to the desired value of M_n when recording the time-domain signal.

Thus, to obtain the transformed radio image from the reference image $<\dot{S}_{21}>$ from the reference $\dot{S}_{21}$ when the antenna is displaced by a distance F along its axis of symmetry, the operator composition $<\dot{S}_{21}> = A\{\Psi\{\dot{S}_{21}\}\}$ is applied.

3. HARDWARE-SOFTWARE SYSTEM FOR REAL-TIME RADAR VISION BASED ON VNA

The radar vision system (Fig. 5) consists of two HE400UW antennas having a range of 0.03–6.0 GHz, as well as a ZNLE6 VNA that has a range of 0.001–6.0 GHz (manufactured by Rohde & Schwarz, Germany).

The peaks in the antenna radiation patterns are mutually aligned at an angle of 60° with a distance of 1 m between the phase centers of the antennas. The VNA is connected to the control computer via Ethernet. The computer runs custom software, whose block diagram is shown in Fig. 6 in the *Simulink* environment.

The generated reference radio images are stored in a database (Block *1*). The SSO radio image under study is received via Block *3* from VNA and fed into Block *2* to calculate the correlation coefficient (CC). Next, the decision-making module (Block *4*) outputs a reference radio image corresponding to the SSO under study. If, based on estimates of the signal-to-noise ratio (SNR) and the signal-to-interference ratio (SIR), the CC value exceeds the 0.9 threshold, the system identifies the SSO.

Figure 7 shows the examples of radio images of SSO (quadcopter) signatures taken from three different angles.

The decrease in amplitude observed in the images is due to frequency-dependent attenuation: high-frequency radio waves are attenuated more rapidly by the environment than low-frequency ones.

Figure 8 shows the VNA screen during real-time recording of an SSO signature radio image.

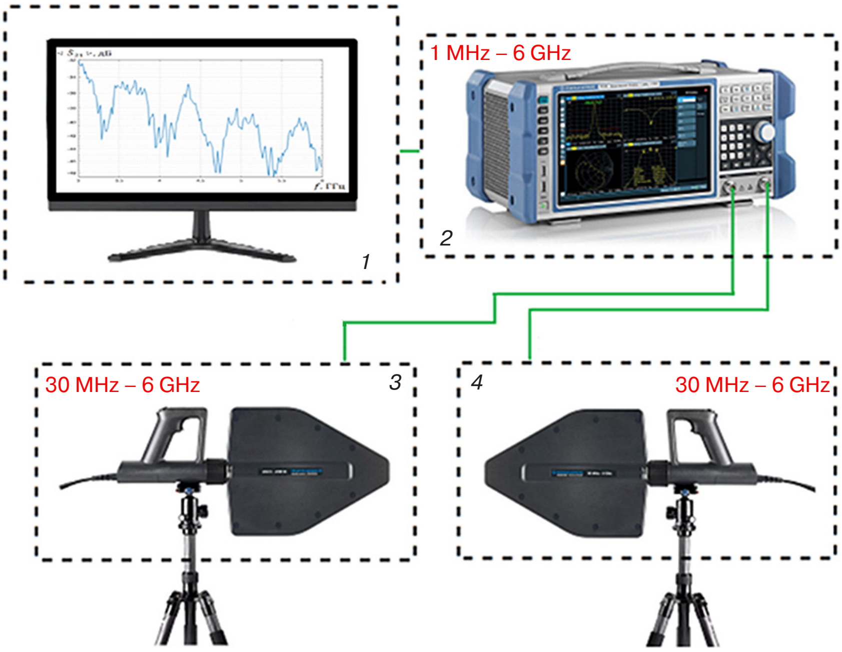

Fig. 5. Block diagram of the real-time radio vision system: (*1*) software implementation in the *Simulink*[2] environment, (*2*) VNA, (*3*) receiving antenna, and (*4*) transmitting antenna

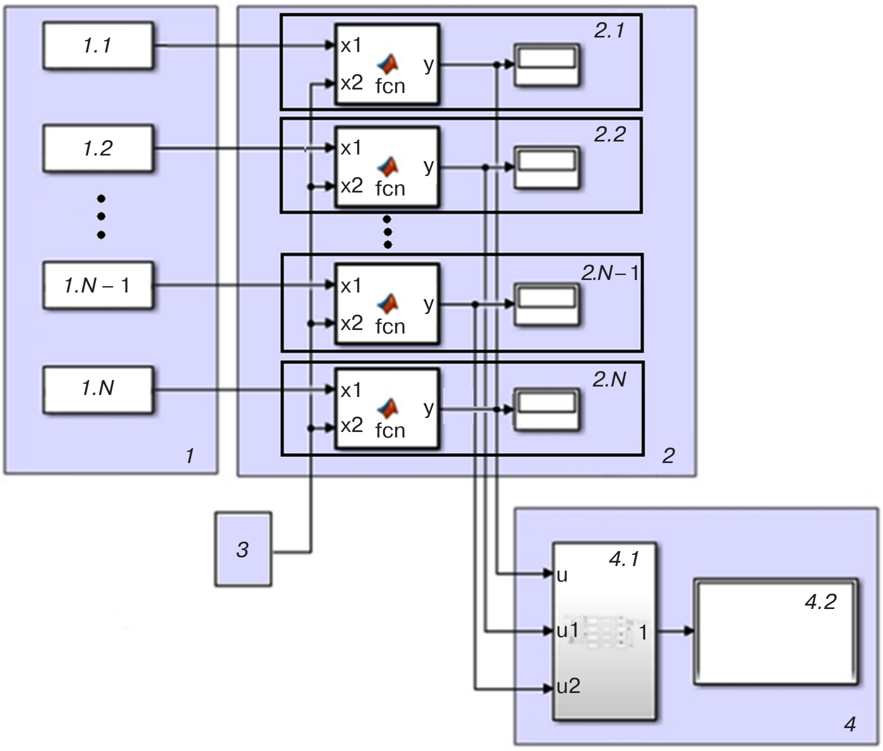

Fig. 6. Block diagram of the radio vision system software suite: (*1*) reference radio image database block (*1.1*, …, *1.N* are reference radio images); (*2*) correlation processing block (*2.1*, …, *2.N* are correlators with graphical output of the correlation coefficient); (*3*) VNA vector data transmission block; (*4*) identification block (*4.1* is the block for finding maximum CC; *4.2* is the module for outputting the name of the corresponding reference radio image); x_1 and x_2 are inputs to the FCN block, in which the correlation of two radio images is compared; u, u_1, and u_2 are inputs of the block *4.1*

[2] https://www.mathworks.com/products/simulink.html. Accessed May 22, 2026.

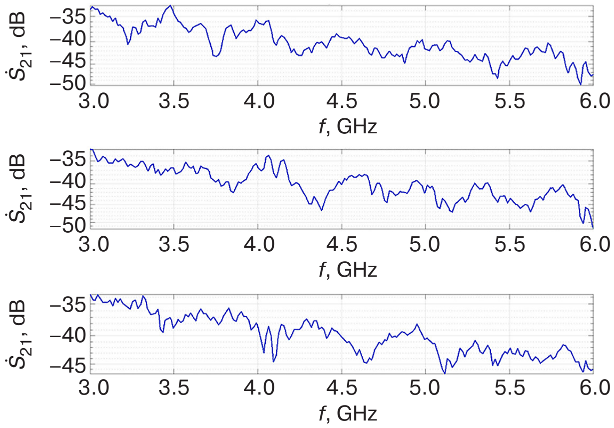

Fig. 7. Radio images of quadcopter-type SSO signatures at three scanning angles: (*1*) 0°, (*2*) 45°, and (*3*) 90°

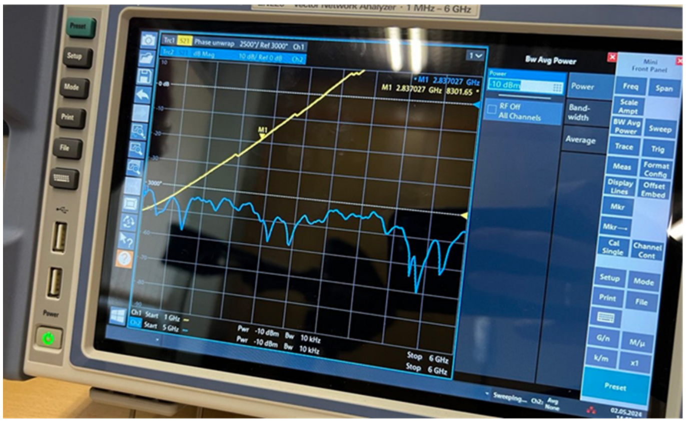

Fig. 8. VNA screen during real-time recording of SSO signature radio images

The radio image of the SSO signature is displayed on the VNA screen as the lower curve. The upper curve shows the phase run-up with the characteristic phase jumps that correspond to the reflection of the radio vision signal from the elementary planes of the SSO signature.

4. EVALUATION OF THE REPRODUCIBILITY OF SSO VECTOR RADIO IMAGES

A series of experiments involving 30 consecutive radio image acquisitions for selected signatures from three SSOs was conducted to evaluate the effectiveness of the method. Imaging performed at three different angles for each object resulted in a sample set of 270 radio images. The proportion of successful identifications was then calculated for each "SSO–angle" combination in the sample. A radio image is considered successful if its CC with the reference image exceeded the 0.9 threshold on the Chaddock scale. Thus, the ratio of successful identifications to the total number of trials was determined for each angular position of each SSO.

According to the Neyman–Pearson criterion, the method's effectiveness, as averaged over the experimental sample for the three SSO signatures and satisfying the CC $\geq$ 0.9 condition, is 95%.

The method's immunity to interference is evaluated by analyzing of the performance of coherent reception when applied to a tracking signal. This is its advantage over pulse-based radio vision [12]. Due to the harmonic nature of the signal, for which the frequency and phase are known at every instant, synthesizing a matched filter becomes a standard problem. The filter's frequency response corresponds to the signal spectrum (up to the coefficient), while its inverse frequency response is the mirror image having a delay equal to the signal duration [13]. Figure 9 shows the spectral representation $|U(f)|$ of the signal accumulated PSD ($N = 200$ harmonics) and interference.

A comparative assessment of the noise immunity of two PSD formation methods is conducted (Fig. 10): impulse (curve *1*) and time-frequency sweep of the PSD (curve *2*) [14]. To this end, the graphs depict the dependence of SNR and SIR on CC of random signatures in the presence of additive white Gaussian noise and non-fluctuating band interference [15].

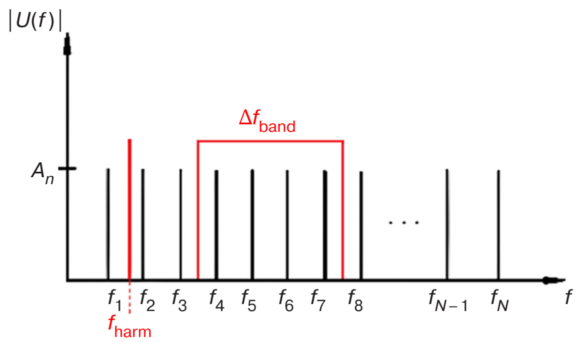

Fig. 9. Synthesized PSD of the signal and PSD of interference: harmonic f_{harm} and band Δf_{band}

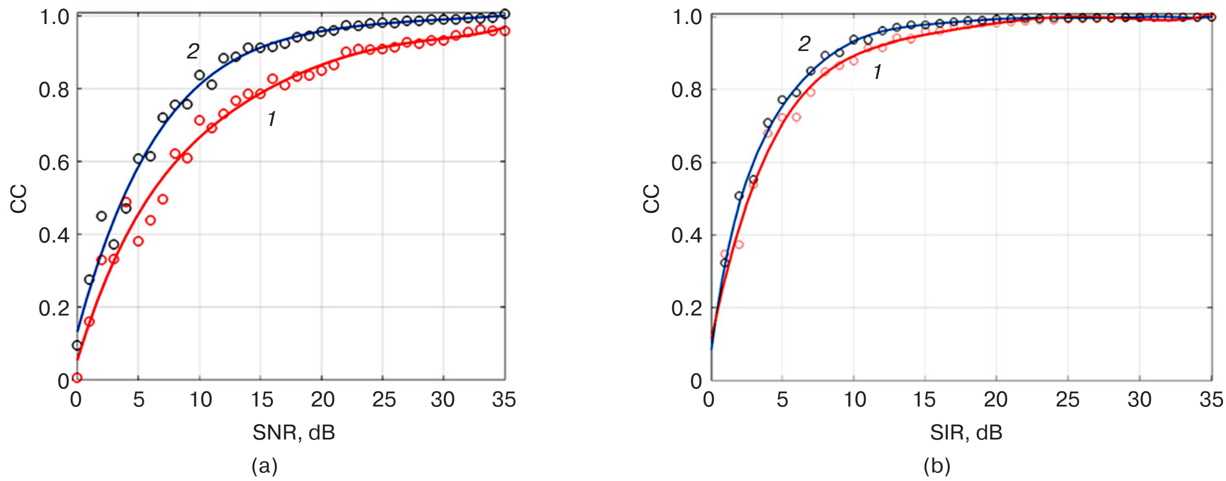

Fig. 10. Distribution of the radio image signature CC as a function of SNR (a) and SIR (b)

The graphs show that, due to coordinated reception, the method for vector tracking-based formation of signal radio image has an advantage of 8 and 5 dB, respectively, compared to pulse radio imaging at CC = 0.9. This ensures SSO verification at SNR ≥ 15 dB and SIR ≥ 9 dB for the time-frequency sweep method, and at SNR ≥ 23 dB and SIR ≥ 14 dB for the pulse-generated PSD method.

CONCLUSIONS

Scientific and practical results regarding the applicability of the tracking-based formation method for verifying vector radio images of SSO signatures have been presented. This was achieved using a radio visualizer laboratory prototype based on a digital VNA (R&S ZNLE6) and two HE400UWB ultra-wideband antennas. The prototype implements a semi-automatic processing cycle in *Simulink* with real-time correlation analysis. The scientific and practical results obtained are as follows:

- The developed method for vector tracking-based formation of signal radio images overcomes the limitations inherent of scalar approaches based on impulse spectrum formation.
- The representation of a heterogeneous radio wave propagation environment has been validated as an *S*-parameter system of coupled *N*-poles, taking into account their spatial orientation.
- The proposed algorithm for the operator Ψ-transform establishes the dependence of projection distortions in vector radio images of signatures on the spatial position of the object.
- It is confirmed that the recognition of SSO signatures based on vector radio images ensures SSO verification at SNR ≥ 15 dB and SIR ≥ 9 dB with a defined CC = 0.9.
- Experimental data confirms reproducible SSO recognition at the 95% level when using a sample of $N \geq 200$ harmonics in coherent radio vision reception at SNR ≥ 15 dB and SIR ≥ 9 dB.

Authors' contribution

The authors' contributions to the preparation of the theoretical section and the conduct of the experiments were distributed equally.

REFERENCES

1. Shadinov S.S. Method of scanning spectral-temporal sweep for obtaining radio images. *Oboronnyi kompleks – nauchno-tekhnicheskomu progressu Rossii = Defense Industry Achievements – Russian Scientific and Technical Progress.* 2024;4(164):57–60 (in Russ.). https://elibrary.ru/bmhwsc
2. Shadinov S.S., Kostin S.S., Konyashkin G.V., Korchagin A.S., Romanovskii M.Y., Gusein-zade N.G. Vector *S*-parametric analysis of signal phase dynamic radio images. *Doklady Rossiiskoi akademii nauk. Fizika, tekhnicheskie nauki = Doklady Physics*. 2023;512(1):78–86 (in Russ.). https://doi.org/10.31857/S2686740023050115
3. Shadinov S.S., Konyashkin G.V. *Program for Capturing and Recognizing Vector Radio Images*: Certificate of State Registration of Computer Program 2025614644 RF. Publ. 25.02.2025 (in Russ.).
4. Kostin M.S., Boikov K.A. Digital technologies of signal radio vision and radio monitoring. *Russian Technological Journal.* 2024;12(4):59–69. https://doi.org/10.32362/2500-316X-2024-12-4-59-69
5. Song S., Lu J., Xing S., et al. Near Field 3D Millimeter-Wave SAR Image Enhancement and Detection with Application of Antenna Pattern Compensation. *Sensors*. 2022;22(1):4509. https://doi.org/10.3390/s22124509
6. Xie Q., Quan X., He B. A Remote Sensing and Meteorological Data-Based Methodology for Wildfire Danger Assessment for China. In: *IGARSS 2020 – 2020 IEEE International Geoscience and Remote Sensing Symposium*. 2020. P. 6798–6801. https://doi.org/10.1109/IGARSS39084.2020.9324063
7. Li X., Li D., Liu H., Wan J., Chen Z., Liu Q. A-BFPN: An Attention-Guided Balanced Feature Pyramid Network for SAR Ship Detection. *Remote Sens.* 2022;14(15):3829–3847. https://doi.org/10.3390/rs14153829
8. Papadopoulos K., Jelali M. A Comparative Study on Recent Progress of Machine Learning-Based Human Activity Recognition with Radar. *Appl. Sci*. 2023;13(23):12728–12761. https://doi.org/10.3390/app132312728
9. Kulikov G.V., Dang X.Kh. Influence of quadrature transformation imbalance on the noise immunity of signal reception with amplitude-phase shift keying. *Russian Technological Journal*. 2024;12(1):59–68. https://doi.org/10.32362/2500-316X-2024-12-1-59-68
10. Yanik M.E., Wang D., Torlak M. Development and Demonstration of MIMO-SAR mmWave Imaging Testbeds. *IEEE Access*. 2020;8:126019–126038. https://doi.org/10.1109/ACCESS.2020.3007877
11. Chen H., Long Z., Niu L., et al. Millimeter-wave SFCW SAR imaging system based on in-phase signal measurement with simplified transceiver. *Opt. Express.* 2020;28(2):1526–1538. https://doi.org/10.1364/oe.380266
12. Kim S., Krieger G., Villano M. Volume Structure Retrieval Using Drone-Based SAR Interferometry with Wide Fractional Bandwidth. *Remote Sens.* 2024;16(8):1352. https://doi.org/10.3390/rs16081352
13. Manzoni M., Tebaldini S., Monti-Guarnieri A.V., et al. Automotive SAR imaging: potentials, challenges, and performances. *Int. J. Microwave Wireless Technol*. 2023;16(1):3–12. https://doi.org/10.1017/S1759078723000326
14. Bolkhovskaya O., Maltsev A., Sergeev V. The wavefront estimation and signal detection in multi-element antenna arrays at low SNR. In: *Proceedings 2018 2nd European Conference on Electrical Engineering and Computer Science* (*EECS*). 2018. P. 497–501. https://doi.org/10.1109/EECS.2018.00097
15. Bolkhovskaya O.V., Maltsev A.A., Sergeev V.A. A passive system for source detection and distance measurement based on signal wavefront estimation. *Radiotekhnika = J. Radioengineering*. 2022;86(9):98–112 (in Russ.). https://doi.org/10.18127/j00338486-202209-11

СПИСОК ЛИТЕРАТУРЫ

1. Шадинов С.С. Метод сканирующей спектрально-временной развертки для получения радиоизображений. *Оборонный комплекс – научно-техническому прогрессу России*. 2024;4(164):57–60. https://elibrary.ru/bmhwsc
2. Шадинов С.С., Костин С.С., Коняшкин Г.В., Корчагин А.С., Романовский М.Ю., Гусейн-заде Н.Г. Векторный *S*-параметрический анализ сигнальных фазодинамических радиоизображений. *Доклады Российской академии наук. Физика, технические науки.* 2023;512(1):78–86. https://doi.org/10.31857/S2686740023050115
3. Шадинов С.С., Коняшкин Г.В. *Программа захвата и распознавания векторных радиоизображений*: Свидетельство о государственной регистрации программы для ЭВМ 2025614644 РФ; опубл. 25.02.2025.
4. Костин М.С., Бойков К.А. Цифровые технологии сигнального радиовидения и радиомониторинга. *Russian Technological Journal*. 2024;12(4):59–69. https://doi.org/10.32362/2500-316X-2024-12-4-59-69
5. Song S., Lu J., Xing S., et al. Near Field 3D Millimeter-Wave SAR Image Enhancement and Detection with Application of Antenna Pattern Compensation. *Sensors*. 2022;22(1):4509. https://doi.org/10.3390/s22124509
6. Xie Q., Quan X., He B. A Remote Sensing and Meteorological Data-Based Methodology for Wildfire Danger Assessment for China. In: *IGARSS 2020 – 2020 IEEE International Geoscience and Remote Sensing Symposium*. 2020. P. 6798–6801. https://doi.org/10.1109/IGARSS39084.2020.9324063
7. Li X., Li D., Liu H., Wan J., Chen Z., Liu Q. A-BFPN: An Attention-Guided Balanced Feature Pyramid Network for SAR Ship Detection. *Remote Sens.* 2022;14(15):3829–3847. https://doi.org/10.3390/rs14153829
8. Papadopoulos K., Jelali M. A Comparative Study on Recent Progress of Machine Learning-Based Human Activity Recognition with Radar. *Appl. Sci*. 2023;13(23):12728–12761. https://doi.org/10.3390/app132312728
9. Куликов Г.В., Данг С.Х. Влияние разбаланса квадратурного преобразования на помехоустойчивость приема сигналов с амплитудно-фазовой манипуляцией. *Russian Technological Journal*. 2024;12(1):59–68. https://doi.org/10.32362/2500-316X-2024-12-1-59-68

10. Yanik M.E., Wang D., Torlak M. Development and Demonstration of MIMO-SAR mmWave Imaging Testbeds. *IEEE Access*. 2020;8:126019–126038. https://doi.org/10.1109/ACCESS.2020.3007877
11. Chen H., Long Z., Niu L., et al. Millimeter-wave SFCW SAR imaging system based on in-phase signal measurement with simplified transceiver. *Opt. Express.* 2020;28(2):1526–1538. https://doi.org/10.1364/oe.380266
12. Kim S., Krieger G., Villano M. Volume Structure Retrieval Using Drone-Based SAR Interferometry with Wide Fractional Bandwidth. *Remote Sens.* 2024;16(8):1352. https://doi.org/10.3390/rs16081352
13. Manzoni M., Tebaldini S., Monti-Guarnieri A.V., et al. Automotive SAR imaging: potentials, challenges, and performances. *Int. J. Microwave Wireless Technol*. 2023;16(1):3–12. https://doi.org/10.1017/S1759078723000326
14. Bolkhovskaya O., Maltsev A., Sergeev V. The wavefront estimation and signal detection in multi-element antenna arrays at low SNR. In: *Proceedings 2018 2nd European Conference on Electrical Engineering and Computer Science* (*EECS*). 2018. P. 497–501. https://doi.org/10.1109/EECS.2018.00097
15. Болховская О.В., Мальцев А.А., Сергеев В.А. Система пассивного обнаружения и измерения расстояния до источника на основе оценки волнового фронта сигнала. *Радиотехника*. 2022;86(9):98–112. https://doi.org/10.18127/j00338486-202209-11

About the Authors

Sergey S. Shadinov, Cand. Sci. (Eng.), Associate Professor, Department of Radio Wave Processes and Technologies, Institute of Radio Electronics and Informatics, MIREA – Russian Technological University (78, Vernadskogo pr., Moscow, 119454 Russia). E-mail: shadinov@mirea.ru. https://orcid.org/0009-0002-3798-5723

Mihail S. Kostin, Dr. Sci. (Eng.), Professor, Head of the Department of Radio Wave Processes and Technologies, Deputy Director, Institute of Radio Electronics and Informatics, MIREA – Russian Technological University (78, Vernadskogo pr., Moscow, 119454 Russia). E-mail: kostin_m@mirea.ru. Scopus Author ID 57208434671, RSCI SPIN-code 5819-2178, http://orcid.org/0000-0002-5232-5478

Об авторах

Шадинов Сергей Семенович, к.т.н., доцент, кафедра радиоволновых процессов и технологий, Институт радиоэлектроники и информатики, ФГБОУ ВО «МИРЭА – Российский технологический университет» (119454, Россия, Москва, пр-т Вернадского, д. 78). E-mail: shadinov@mirea.ru. https://orcid.org/0009-0002-3798-5723

Костин Михаил Сергеевич, д.т.н., профессор, заведующий кафедрой радиоволновых процессов и технологий, заместитель директора Института радиоэлектроники и информатики, ФГБОУ ВО «МИРЭА – Российский технологический университет» (119454, Россия, Москва, пр-т Вернадского, д. 78). E-mail: kostin_m@mirea.ru. Scopus Author ID 57208434671, SPIN-код РИНЦ 5819-2178, http://orcid.org/0000-0002-5232-5478

Translated from Russian into English by K. Nazarov
Edited for English language and spelling by Thomas A. Beavitt